Publisher: GSA
Journal: GEOL: Geology
DOI:10.1130/G39181.1

Earthquake nucleation on rough faults

Christopher W.A. Harbord, Stefan B. Nielsen, Nicola De Paola, and Robert E. Holdsworth

Rock Mechanics Laboratory, Department of Earth Sciences, Durham University, South Road, Durham DH1 3LE, UK

ABSTRACT

Earthquake nucleation is currently explained by rate-and-state stability analysis, which successfully models the behavior of laboratory simulated faults with constant thickness gouge layers. However roughness is widely observed on natural faults and its influence on earthquake nucleation is little explored. Here we conduct frictional sliding experiments with different roughnesses on granite samples at upper crustal conditions (30–200 MPa). We observe a wide range of behaviors, from stable sliding to stick-slip, depending on the combination of roughness parameters and normal stress. Stick-slip is repeatedly observed in velocity-strengthening regimes, and increases in normal stress stabilize slip; these features are not fully predicted by current stability analysis. We derive a new instability criterion which matches our observations, based on fracture energy considerations and the size of weak patches created by fault roughness.

INTRODUCTION

A central question regarding tectonic faults concerns the onset of earthquake-generating stick-slip as opposed to aseismic stable sliding. This problem has been addressed in observational (Dodge et al., 1996), theoretical (Rice and Ruina, 1983) and experimental studies (Leeman et al., 2016; Scuderi et al., 2016) using the predictions of rate-and-state friction law and stability analysis, where instability develops under velocity-weakening friction and low mechanical stiffness (Leeman et al., 2016; Marone, 1998; Scuderi et al., 2016). However, most experiments have been conducted on homogeneous materials, either generating slip in a constant thickness gouge layer e.g. (Leeman et al., 2016; Scuderi et al., 2016) or on roughened cohesive rock surfaces e.g. (Passelegue et al., 2013). Natural faults, on the other hand, are highly heterogeneous features with variable composition, physical properties and complex slip surface geometries (Bistacchi et al., 2011; Brodsky et al., 2016; Candela et al., 2012; Sagy et al., 2007).

In this study we investigate the effects of heterogeneity due to the roughness of fault surfaces, and its influence on the onset of unstable sliding. Roughness is observed on faults at all scales (Bistacchi et al., 2011; Candela et al., 2012; Sagy et al., 2007), and plays a key role in fault mechanics by determining the size and distribution of asperities (Dieterich and Kilgore, 1994; Scholz, 1988), which control the stress distribution on the fault surface (Persson, 2013; Selvadurai and Glaser, 2017). It is therefore argued that roughness should have significant implications for both the static (Brodsky et al., 2016) and dynamic frictional strength of fault zones (Fang and Dunham, 2013), critical slip distances (Candela and Brodsky, 2016; Ohnaka and Shen, 1999; Okubo and Dieterich, 1984), and nucleation size (Ohnaka and Shen, 1999; Okubo and Dieterich, 1984). Currently only a narrow range of conditions have been investigated experimentally (Marone and Cox, 1994; Ohnaka and Shen, 1999; Okubo and Dieterich, 1984).

Here we report results of the first systematic experimental study investigating the occurrence of frictional instability under a range of roughness and normal stress conditions. We show that the combination of these parameters controls the onset of frictional instability of faults. We then provide a novel explanation based on the interaction between maximum weak patch scaling, roughness and normal stress.

METHODS

We performed 23 frictional sliding experiments with Westerly granite subjected to stress conditions representative of the Earth's upper crust (30 MPa ≤ σ_n ≤ 200 MPa) and loaded in a direct shear configuration to force sliding. Samples were subjected to an initial period of 1-1.5 mm run-in before carrying out a sequence of velocity steps between 0.1-10 μm s^{-1}. To create different distributions of heterogeneity on the simulated faults, the sliding surfaces were axially pre-cut and carefully polished to obtain variable degrees of roughness, characterized in terms of root mean square roughness (Z_{rms}) using stylus profilometry measurements (see SM1 and SM2).

RESULTS

All experiments show initial elastic loading followed by frictional roll-over where the contacting surfaces begin to slide (see Figure 1 and summary of results in SM3 and SM4, respectively). Once past this initial stage, the frictional strength remains relatively constant and a steady-state is reached (typically requiring a displacement of 0.75–1.5 mm). The full spectrum of frictional sliding behaviors is observed, from stable sliding to seismic stick-slip, across the range of experimental conditions. In several experiments, it was possible to determine the rate-and-state friction parameters *a, b* by modeling the frictional data to load-point velocity stepping during stable sliding episodes (SM3). Figure 1 shows examples of typical slip dynamics observed in different experiments (full plots in SM3).

At lower normal stress (σ_n = 30 MPa), rougher faults ($Z_{rms} \geq 8$ μm) are observed to slide stably with velocity-neutral friction (Fig. 1a). Velocity weakening friction and marginal stability is confined to the smoothest faults ($Z_{rms} \leq 4.3$ μm), manifested by fast stress drops during step-wise velocity increases (Fig. 1b).

When normal stress is increased to 100 MPa, smooth faults ($Z_{rms} \leq 4.3$ μm) are observed to become fully unstable with repetitive fast stick-slip instabilities (Fig. 1c). This behavior is confirmed by observations of frictional melting in scanning electron microscopy (SEM) imaging of slip surfaces (Fig. 2c, SM5). Intermediate roughness surfaces (Z_{rms} = 8 μm) show marginal stability with velocity-weakening to neutral friction accompanied by slow stress drops upon increases in velocity (Fig. 1d). Rougher faults ($Z_{rms} \geq 18.4$ μm), are stable throughout the course of experimentation with velocity-strengthening friction, and abundant cataclasis observed in SEM imaging (Fig. 2d, SM5).

For σ_n > 100 MPa sliding shows a wider spectrum of behaviors, with some unexpected results. At 150 MPa smooth faults ($Z_{rms} \leq 4.3$ μm) remain unstable with repetitive fast stick-slip cycles. Suprisingly, all rougher faults (Z_{rms} > 4.3 μm) are marginally stable, with evidence of fast stress drops nucleating spontaneously (without a velocity kick) or upon step-wise velocity increases, in spite of velocity-strengthening friction measurements (Fig. 1e, SM3 and SM4), and evidence of frictional melt in SEM images (Fig. 1b, SM5). Surprisingly increasing the normal stress to 200 MPa results in the smoothest faults ($Z_{rms} \leq 4.3$ μm) becoming marginally stable (Fig. 1f). Similar behavior is also observed on intermediate roughness faults (4.3 < Z_{rms} < 28.2 μm) which are stable with velocity-neutral to -strengthening friction. Unexpectedly, given the

DOI:10.1130/G39181.1

consistently velocity-strengthening friction at lower normal stresses, the roughest fault (Z_{rms} = 28.2 μm) is unstable with repetitive dynamic stick-slip (SM3).

The complex variety of slip behaviors observed is summarized in Figure 2A, where points correspond to various experimental conditions (Z_{rms}, σ_n), which allow approximate definition of differing frictional domains. Two characteristic trends emerge in the data (Fig. 2): First, there is a transition from stable to unstable and marginally stable slip as normal stress is increased, in accordance with the predictions of rate and state (Marone, 1998; Rice and Ruina, 1983), with the transition at increasingly higher normal stress as faults become rougher. Secondly, with further normal stress increase up to 200 MPa, instability is suppressed on all but the roughest fault which becomes unstable (Fig. 2a). The occurrence of spontaneous rupture nucleation in a velocity strengthening regime for several experiments and the second trend of the stabilizing effect of normal stress are not predicted using a standard stability analysis (Marone, 1998; Rice and Ruina, 1983).

DISCUSSION

We now discuss these results in light of rupture stability criteria and develop a theoretical model based on roughness-induced weak fault patches. To frame the following discussion we must first consider surface roughness statistics. Studies of natural fault surfaces show that faults have a characteristic self-affine roughness, described by a power density spectrum

$$P(k) = \alpha \left(\frac{k}{k_0}\right)^{-1-2H} \quad (1)$$

where α is the amplitude scaling in m^3, k the inverse wavelength in m^{-1}, H the Hurst exponent and k_0 a normalizing factor (here 1 m^{-1}). Results suggest that this is true over 9-orders of magnitude (from $10^{-4}$to 10^5 m) with $\alpha = 10^{-3} - 10^{-1}$ m^3 and $H = 0.6 - 0.8$ (Bistacchi et al., 2011; Candela et al., 2012). At shorter length scales of <1–50 μm, this scaling diminishes and becomes isotropic as a result of plastic yielding at asperity contacts (Candela and Brodsky, 2016). From stylus profilometry measurements of our pre- and post-experimental surfaces we have a inverse corner wavelength, k_{min}, identified using Fourier analysis (see SM2), above which surfaces obey self-affine scaling. The power law parameters and k_{min} can be related to the root mean square of elevation such that $Z_{rms} = \sqrt{\frac{\alpha k_0}{2H}} \left(\frac{k_{min}}{k_0}\right)^{-H}$ (SM6). Therefore, Z_{rms} is selected as a single representative parameter of the surface statistics in Figure 2, and throughout the following discussion.

The onset of rupture propagation can be interpreted either: (a) in the context of rate- and state-dependent friction (Marone, 1998; Rice and Ruina, 1983), when stable sliding initiating at a point can spread out with an accelerating velocity when the sliding patch reaches a critical size or (b) as the consequence of stress concentration around a weak patch, which may propagate unstably according to fracture energy considerations, originally developed in fracture mechanics (Griffith, 1921), which have been adapted to the problem of shear cracks and earthquake faulting (Andrews, 1976; Ida, 1972) .

According to criterion (a), stability is controlled by the ratio of the mechanical stiffness K_f to the frictional stiffness K_c, defined as $K_c = \frac{\sigma_n(b-a)}{D_c}$, where σ_n is the normal stress, a and b are rate- and state-friction dimensionless parameters and D_c is the critical slip distance with dimensions of length. When the stiffness criterion $\frac{K_f}{K_c} < 1$ is satisfied, instability can develop, otherwise sliding is conditionally stable (Marone, 1998; Rice and Ruina, 1983). In the case of tectonic faults embedded in an elastic medium, K_f represents the stiffness of the fault and can be expressed as $K_f = C\frac{G}{h}$, where G is the shear modulus, h the linear fault dimension and C is a dimensionless shape factor (Rubin and Ampuero, 2005). The stiffness criterion allows definition of the minimum dimension h*

$$h^* = C\frac{GD_c}{\sigma_n(b-a)} \quad (2)$$

of a slip patch required for instability to develop. Rate- and state-friction laws and Equation 2 provide effective tools to model slip during the earthquake cycle. The stiffness criterion has been successfully used to explain the spectrum of fault slip behaviors observed across relative homogeneous sliding interfaces such as gouge dominated faults (Leeman et al., 2016; Scuderi et al., 2016).

On the other hand, stability criterion (b) based on fracture energy, surmises the presence of a pre-existing flaw or weak patch of finite size. Material flaws are inherent in Griffith's original crack theory (Griffith, 1921), and in the case of tectonic faults we may equate them to an elastic bridge between asperities (Fig. 3a-b). For earthquake nucleation, instability arises when the growth of the weak patch is energetically favorable, requiring that the strain energy release balances or exceeds the work done against residual strength.

In problems of shear crack propagation, fracture energy is often equated to the frictional work dissipated during the loss of strength, according to a model of slip weakening, over a characteristic distance, δ_c (Andrews, 1976; Ida, 1972). Typically δ_c is taken to represent the dynamic weakening distance, however here we use it to represent a weakening distance at low velocity.

Criterion (b) allows the definition of a critical length, $L_c = C' G \delta_c \frac{\tau_p - \tau_r}{(\tau_0 - \tau_r)^2}$ at which a shear crack undergoes unstable dynamic failure (Andrews, 1976), where C is a dimensionless shape factor, τ_0, is the static shear stress on the fault, $\tau_p = \mu_p \sigma_n$ is the peak stress, μ_p the peak friction coefficient and $\tau_r = \mu_r \sigma_n$ is the shear stress after weakening where μ_r is the sliding or weak friction coefficient. To enhance similarity with h^* (Equation 2), we derive a lower bound length estimate for L_c by assuming that the stress state on the fault is close to the peak stress during experiments (i.e., $\tau_0 \approx \tau_p$), yielding

$$L_c \approx C' \frac{G \delta_c}{\sigma_n \left(\mu_p - \mu_r\right)} (3)$$

Though the critical patch length h^* and L_c share some scaling similarities, they may differ by orders of magnitude. Indeed, $a - b$ is usually small (typically –0.01) while we can expect $\mu_p - \mu_r$ can be quite large (> 0.1) within weak patches between frictional asperities (Selvadurai and Glaser, 2017). Here the frictional strength at asperities equates to μ_p, and within elastic bridges or zones of reduced asperity density equivalent to μ_r as is supported by the observations of Selvadurai and Glaser (2017), which show stress fluctuations can be up to 40% of the peak stress.

Estimates of nucleation size for experiments showing stick-slip instability at moderate normal stress using Equation 2 for a fault of Z_{rms} = 3.6 μm (a-b = –0.003, D_c = 5μm, G = 50 GPa (estimated from loading curves), σ_n = 100 MPa) yield h^* values of around a meter, about two orders of magnitude larger than the size of samples utilized.

DOI:10.1130/G39181.1

Following Rubin and Ampuero (2005) if we neglect the rate parameter a, we find h_b^* reduces by a factor of 3 (a = 0.005), which is still an order of magnitude larger than the size of the sample. If we calculate the nucleation length using Equation 3, we obtain $L_c = 1.25 - 3.75$ cm (with G = 50 GPa (estimated from loading curves), σ_n = 100 MPa, μ_p - μ_r = 0.2 (following Selvadurai and Glaser (2017))) and δ_c = 5 – 15 μm). Values of L_c obtained are in agreement with other studies that posit that the nucleation length should be smaller than the sample length (L_0 = 4 cm), for lab stick-slip occurrence (Ohnaka and Shen, 1999; Okubo and Dieterich, 1984; Passelegue et al., 2013). The values estimated here for $\delta_c = 0.05\ k_{min}^{-1}$ (Ohnaka and Shen, 1999) are consistent with previous estimates using high frequency strain gauges (Okubo and Dieterich, 1984) and also those predicted by numerical modeling of elastic surface closure (see SM7). This is in contrast to values of D_c obtained during velocity steps, which do not show a systematic dependence on roughness. The onset of instability observed at higher normal stress for increasing roughness is in accord with $\delta_c \propto k_{min}^{-1}$, as larger values of Z_{rms} equate to larger values of k_{min}^{-1} and therefore larger δ_c.

While a stability criterion based on fracture energy (e.g., Equation 3) can explain the onset of stick-slip during our experiments at low/moderate normal stresses (30–150 MPa), the surprising observation that slip instability is suppressed at higher normal stress indicates the presence of some limiting process (Fig. 2A). As we discuss below, this behavior could be explained by considering the microphysical properties of contact asperity distribution in relation to fault zone roughness, and the associated stress heterogeneity (Scholz, 1988).

Previous studies imaged the distribution of frictional contacts with increasing normal stress and varying surface roughness in transparent materials (Dieterich and Kilgore, 1994; Selvadurai and Glaser, 2017). With increasing normal stress, contact asperities increase in number and also grow as is shown in figure 3 (SM6). Theory indicates that stress and asperity sizes will follow a power law distribution for a self-affine surface under load (Scholz, 1988). The asperity bridging length, λ_c, which is the maximum supportable elastic length or bridge between asperities, is also shown to decrease as $\lambda_c \propto {\sigma_n}^{-2}$ for a self-similar surface (Scholz, 1988). Here we consider a generalization of this result to any self-affine surface with $0 < H < 1$ as

$$\lambda_c = \beta \left(\frac{G}{\sigma_n}\right)^{\frac{1}{1-H}} \quad (4)$$

where $\beta = \left(\sqrt{\frac{\alpha {k_0}^{(1+2H)}}{2H}}\right)^{\frac{1}{1-H}}$ is a scaling factor of length dimension (SM6). From measurements of experimental fault surfaces, the Hurst exponent is typically 0.6–0.9 above k_{min}, yielding $\lambda_c \propto {\sigma_n}^{-2.5} - {\sigma_n}^{-10}$. In comparison, Equation 3 gives $L_c \propto {\sigma_n}^{-1}$, demonstrating that as normal stress increases, the bridging length will decrease at a faster rate than that of the nucleation length (Fig. 4). In extreme cases, bridges of length scale λ_c may represent voids, as is shown in figure 3, but more generally zones of reduced normal stress, or weak patches of low stiffness, filled with under-compacted gouge. These weak zones can act as stress concentrators and initiate rupture, provided that $L_c < \lambda_c$ as is shown in figure 4. However with increasing normal stress, the bridges will gradually be closed and the maximum open patch will decrease until $\lambda_c < L_c$, and rupture nucleation is no longer possible in accordance with our experimental observations (Fig. 2). In

Publisher: GSA
Journal: GEOL: Geology
DOI:10.1130/G39181.1

general, instability leading to rupture nucleation in our experiments is only observed when the nucleation length L_c satisfies the condition $\lambda_c > L_c$ and $L_0 > L_c$. Conversely the conditions $L_c > L_0$ at lower normal stress, and $L_c > \lambda_c$ at higher normal stress, lead to stable sliding (Fig. 4).

CONCLUSIONS

Our findings also have implications for the larger scale behavior of natural fault zones. In principle, the model shown in Figure 4 suggests the transition from seismic to aseismic faulting may possibly be controlled by the stabilizing influence of increasing normal stress upon asperities as originally suggested by Brace and Kohlstedt (1980), in addition to currently accepted temperature-induced rheological changes (Scholz, 1988). In addition to this our results qualitatively support observations of subduction zone seismicity, where rough sea floor topography is observed to be related to creeping behavior, and smooth sea floor topography to seismicity and large earthquake nucleation (Wang and Bilek, 2014). We speculate that the close spacing of sea mounts may act as a nucleation buffer in a similar manner to the model proposed here due to the stabilizing effects of increased asperity density.

Our results highlight the key role of fault heterogeneity in earthquake nucleation, which suggests that on larger scales earthquakes are likely to be triggered by heterogeneous fault structure and characteristics, e.g. fault jogs, compositional contrasts, fluid injection or, as in the case argued in this paper, fault roughness. These results complement rate-and-state friction stability analysis, providing a physical framework to include the complexity of roughness in earthquake nucleation models.

ACKNOWLEDGEMENTS

CH acknowledges NERC studentship 1483318 and SN NERC HiFASt grant. We are grateful to Eric Dunham and two anonymous reviewers which significantly helped to clarify the manuscript. Cyril Bourgenot and Ian Chaplain are thanked for their technical support.

REFERENCES CITED

Andrews, D. J., 1976, Rupture velocity of plane strain shear cracks: Journal of Geophysical Research, v. 81, no. 32, p. 5679-5687.

Bistacchi, A., Griffith, W. A., Smith, S. A. F., Di Toro, G., Jones, R., and Nielsen, S., 2011, Fault Roughness at Seismogenic Depths from LIDAR and Photogrammetric Analysis: Pure and Applied Geophysics, v. 168, no. 12, p. 2345-2363.

Brace, W. F., and Kohlstedt, D. L., 1980, Limits on lithospheric stress imposed by laboratory experiments: Journal of Geophysical Research: Solid Earth, v. 85, no. B11, p. 6248-6252.

Brodsky, E. E., Kirkpatrick, J. D., and Candela, T., 2016, Constraints from fault roughness on the scale-dependent strength of rocks: Geology, v. 44, no. 1, p. 19-22.

Candela, T., and Brodsky, E. E., 2016, The minimum scale of grooving on faults: Geology, v. 44, no. 8, p. 603-606.

Candela, T., Renard, F., Klinger, Y., Mair, K., Schmittbuhl, J., and Brodsky, E. E., 2012, Roughness of fault surfaces over nine decades of length scales: Journal of Geophysical Research-Solid Earth, v. 117, p. 30.

Dieterich, J. H., and Kilgore, B. D., 1994, Direct observation of frictional contacts - new insights for state-dependent properties: Pure and Applied Geophysics, v. 143, no. 1-3, p. 283-302.

Dodge, D. A., Beroza, G. C., and Ellsworth, W. L., 1996, Detailed observations of California foreshock sequences: Implications for the earthquake initiation process: Journal of Geophysical Research: Solid Earth, v. 101, no. B10, p. 22371-22392.

Fang, Z. J., and Dunham, E. M., 2013, Additional shear resistance from fault roughness and stress levels on geometrically complex faults: Journal of Geophysical Research-Solid Earth, v. 118, no. 7, p. 3642-3654.

Griffith, A. A., 1921, The phenomena of rupture and flow in solids: Philosophical transactions of the royal society of london. Series A, containing papers of a mathematical or physical character, v. 221, p. 163-198.

Ida, Y., 1972, Cohesive force across tip of a longitudinal-shear crack and griffiths specific surface-energy: Journal of Geophysical Research, v. 77, no. 20, p. 3796-&.

Leeman, J., Saffer, D., Scuderi, M., and Marone, C., 2016, Laboratory observations of slow earthquakes and the spectrum of tectonic fault slip modes: Nature communications, v. 7.

Marone, C., 1998, Laboratory-derived friction laws and their application to seismic faulting: Annual Review of Earth and Planetary Sciences, v. 26, p. 643-696.

Marone, C., and Cox, S. J. D., 1994, Scaling of rock friction constitutive parameters - the effects of surface-roughness and cumulative offset on friction of gabbro: Pure and Applied Geophysics, v. 143, no. 1-3, p. 359-385.

Ohnaka, M., and Shen, L.-f., 1999, Scaling of the shear rupture process from nucleation to dynamic propagation: Implications of geometric irregularity of the rupturing surfaces: Journal of Geophysical Research: Solid Earth, v. 104, no. B1, p. 817-844.

Okubo, P. G., and Dieterich, J. H., 1984, Effects of physical fault properties on frictional instabilities produced on simulated faults: Journal of Geophysical Research, v. 89, no. NB7, p. 5817-5827.

Passelegue, F. X., Schubnel, A., Nielsen, S., Bhat, H. S., and Madariaga, R., 2013, From Sub-Rayleigh to Supershear Ruptures During Stick-Slip Experiments on Crustal Rocks: Science, v. 340, no. 6137, p. 1208-1211.

Persson, B., 2013, Sliding friction: physical principles and applications, Springer Science & Business Media.

Rice, J. R., and Ruina, A. L., 1983, Stability of steady frictional slipping: Journal of Applied Mechanics-Transactions of the Asme, v. 50, no. 2, p. 343-349.

Rubin, A. M., and Ampuero, J. P., 2005, Earthquake nucleation on (aging) rate and state faults: Journal of Geophysical Research: Solid Earth, v. 110, no. B11, p. n/a-n/a.

Sagy, A., Brodsky, E. E., and Axen, G. J., 2007, Evolution of fault-surface roughness with slip: Geology, v. 35, no. 3, p. 283-286.

Scholz, C. H., 1988, The critical slip distance for seismic faulting: Nature, v. 336, no. 6201, p. 761-763.

Scuderi, M. M., Marone, C., Tinti, E., Di Stefano, G., and Collettini, C., 2016, Precursory changes in seismic velocity for the spectrum of earthquake failure modes: Nature Geosci, v. 9, no. 9, p. 695-700.

Selvadurai, P. A., and Glaser, S. D., 2017, Asperity generation and its relationship to seismicity on a planar fault: a laboratory simulation: Geophysical Journal International, v. 208, no. 2, p. 1009-1025.

Wang, K., and Bilek, S. L., 2014, Invited review paper: Fault creep caused by subduction of rough seafloor relief: Tectonophysics, v. 610, p. 1-24.

FIGURES

DOI:10.1130/G39181.1

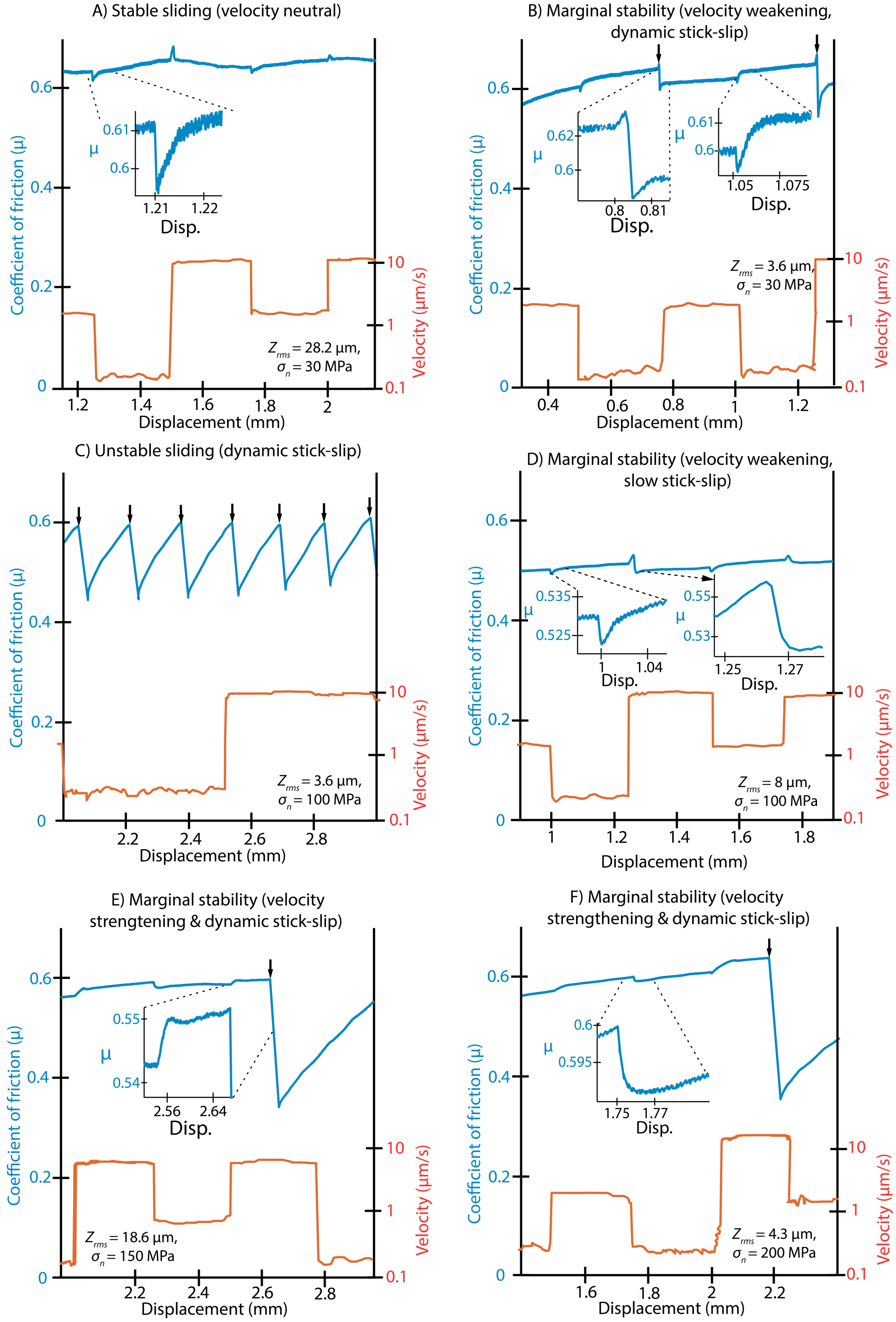

Figure 1. Spectrum of frictional sliding behaviors as a result of varying roughness and normal stress, see text for description of individual experiments (full plots in SM3).

Publisher: GSA
Journal: GEOL: Geology
DOI:10.1130/G39181.1

312 Zoomed plots show examples of velocity steps and stress drops, arrows indicate the onset

313 of dynamic stick-slip.

314

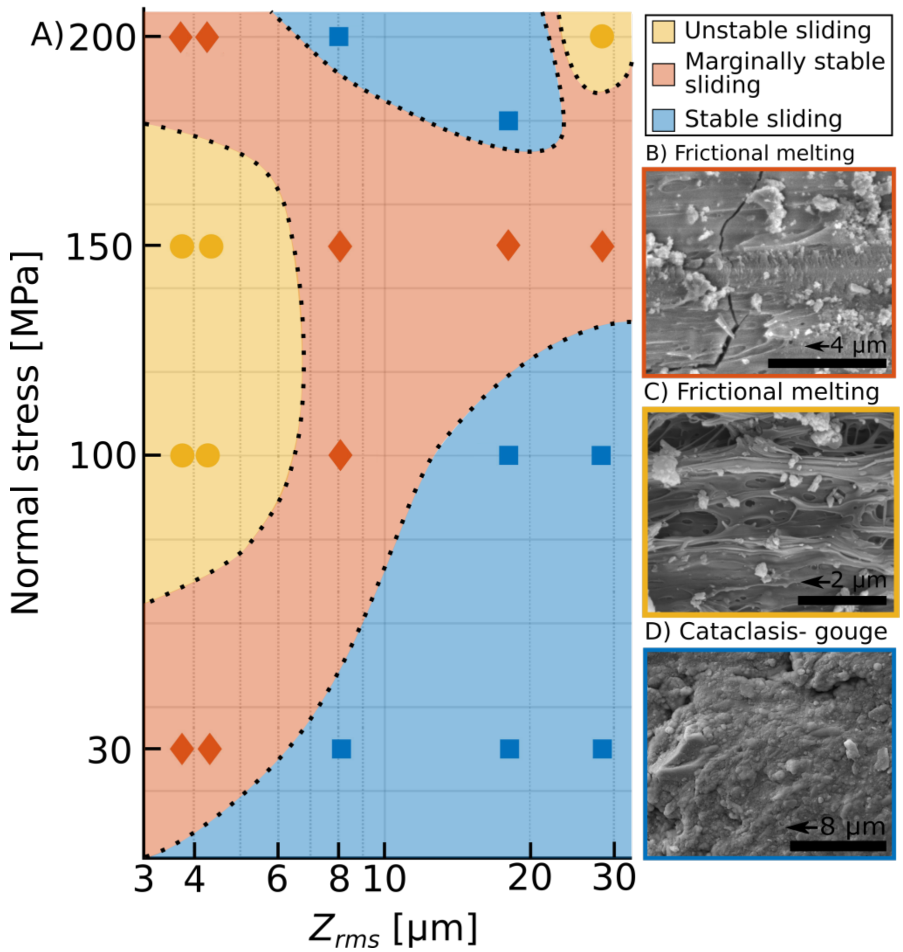

315 Figure 2. A) Map of frictional stability regimes. Each point represents an individual

316 experiment; boundaries have been added to enhance trends and are drawn at the midpoint

317 between data points. Inset SEM images represent characteristic microstructures of each

318 domain (B) marginal stability, C) unstable sliding, D) stable sliding).

Publisher: GSA
Journal: GEOL: Geology
DOI:10.1130/G39181.1

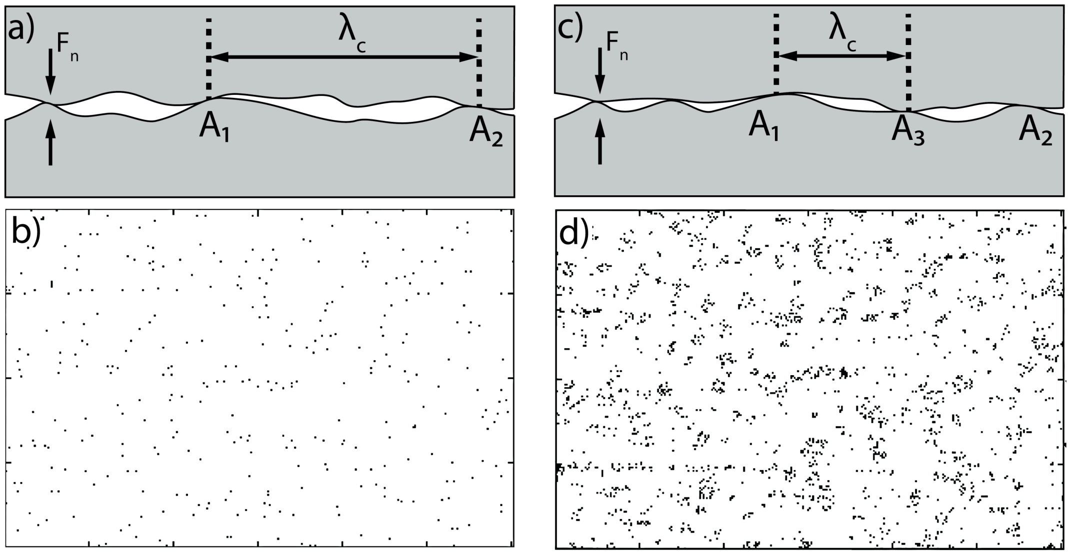

319

320 Figure 3. Schematic illustration of $\lambda_{c,}$ the bridging length in cross-section in insets A) and
321 B), which is the characteristic scaling between frictional asperities (A_n). Insets C) and D)
322 represent frictional contact in map view from an elastic model of frictional contact. Insets
323 A) and C) represent frictional contact at low normal stress, and B) and D) and high
324 normal stress, indicating that as load increases the spacing between asperities decreases
325 due to asperity multiplication (see SM7 for details of modeling).

DOI:10.1130/G39181.1

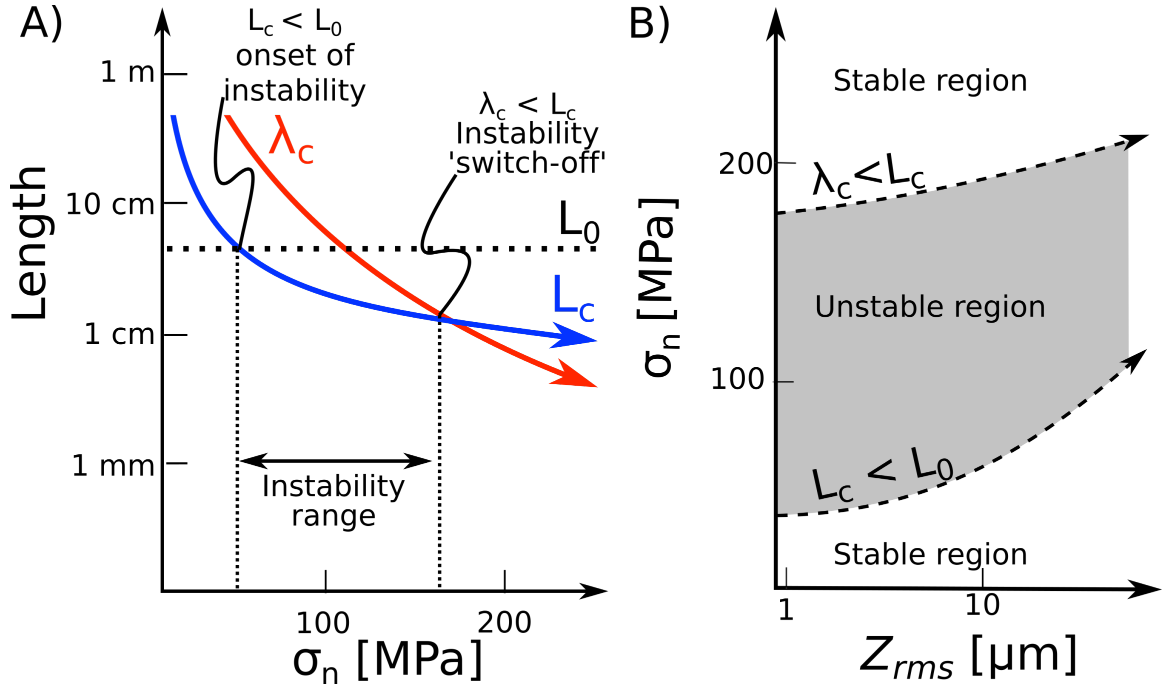

Figure 4. Inset A) schematic illustration of dimensional argument proposed to explain experimental results and inset B) the predicted regimes of frictional sliding.

1GSA Data Repository item 2017xxx, xxxxxxxx, is available online at http://www.geosociety.org/datarepository/2017/ or on request from editing@geosociety.org.